

**Signatures of the spin-triplet current in a Josephson spin valve: A micromagnetic analysis**

Adrian Iovan and Vladimir M. Krasnov

*Department of Physics, Stockholm University, AlbaNova University Center, SE-10691 Stockholm, Sweden*

(Received 23 May 2017; published 18 July 2017)

A Josephson spin valve is a ferromagnetic spin valve sandwiched between two superconducting electrodes. It has been predicted theoretically that such a device may exhibit a long-range proximity effect due to generation of unconventional odd-frequency spin-triplet and long-range spin-singlet components of the supercurrent. In this work we present a comprehensive numerical analysis of Josephson spin-valve characteristics. Our analysis is based on micromagnetic simulations for Ni-based spin valves. The supercurrent through the spin valve depends on shapes and sizes of components, the magnetic domain structure, and the flux quantization. For very small monodomain spin valves, the triplet current is manifested by a dissimilar double maximum in the magnetic field dependence of the critical current  $I_c(H)$ . However, this feature is washed away in larger devices due to appearance of domains and flux quantization. The only remaining signature of the triplet current in this case are beatings in  $I_c(H)$  with a half-flux quantum periodicity. The complexity of the device can make it difficult to identify the spin-triplet supercurrent without a detailed knowledge of the spin-valve state. However, we argue that unambiguous conclusions can be made from a systematic analysis of size, thickness, and shape dependencies of the Josephson spin-valve characteristics.

DOI: [10.1103/PhysRevB.96.014511](https://doi.org/10.1103/PhysRevB.96.014511)**I. INTRODUCTION**

A competition between ferromagnetic (F) and superconducting (S) orders in hybrid S/F heterostructures leads to a variety of unusual physical phenomena [1–15]. Perhaps, most interesting is a possibility of controllable generation of unconventional odd-frequency spin-triplet [2,7] and long-range spin-singlet [10] components of the superconducting condensate, which are immune to a strong exchange field in a ferromagnet and should lead to a long-range proximity effect through F layers, as reported in several experiments [16–21]. However, the spin-triplet order parameter in F is generated only in presence of spin-active interfaces [5,7], or spatially nonuniform case with a noncollinear magnetization [2]. It is not obvious how to do this in a controllable manner for a single-F layer. On the other hand, a noncollinear magnetic state can be easily achieved in a spin-valve structures with several F layers. The long-range supercurrent in such S/F multilayers depends on relative angles between magnetizations of adjacent F layers [1,3,6,8,10,11,22].

The Josephson spin valve (JSV) is the simplest device that allows controllable generation of the spin-triplet component of a supercurrent. JSV has a spin valve with two ferromagnetic layers  $F_{1,2}$  imbedded as a barrier in a Josephson junction, thus having a structure  $SF_1F_2S$ . According to Mel'nikov and co-workers [10], the Josephson current through the JSV has three main components: a conventional short-range spin singlet, an unconventional long-range spin singlet, and a long-range spin triplet. The long-range spin-singlet current is at maximum for the antiparallel state of the spin valve  $\alpha = \pi$  [10] and the spin-triplet component is at maximum in the noncollinear state  $\alpha = \pi/2$  [8]. Here,  $\alpha$  is the relative angle between magnetizations of the two F layers. The amplitudes of different current components depend on F-layer properties in the following way: the short-scale singlet decreases rapidly with increasing the thickness of both  $F_{1,2}$  layers. The amplitude of the long-range singlet current is at maximum in the symmetric JSV with identical layers  $F_1 = F_2$  because this leads to cancellation of the exchange field in

the antiparallel state [4,10]. On the contrary, the long-range triplet is proportional to the difference between  $F_1$  and  $F_2$  [8]. Therefore, an asymmetric JSV  $F_1 \neq F_2$  is needed for generation of the spin-triplet current. The asymmetry (different coercive fields) is also useful for controllable tuning of the relative magnetization angle  $\alpha$  in the spin valve.

Although the supercurrent has been observed in Josephson spin valves [23–28] and more complex S/F heterostructures [29,30], a conclusive evidence for spin-triplet nature of the supercurrent and quantification of the singlet and triplet components is still missing. The difficulty of interpretation is caused by the complexity of JSV devices with many coexisting phenomena. The supercurrent is very sensitive to the F-layer thickness [4,28,31], the electronic mean-free path: clean versus dirty case [32]. This requires nm-scale control of layer roughness and uniformity [33], as well as control of film structure and composition. The Josephson current in JSV is influenced by stray fields, flux quantization in the junction (Josephson vortices) [34,35], and Abrikosov vortices in electrodes [36,37] and by domain configuration of magnetization in F layers [26,30,38], which is hard to control. Magnetic state of the spin valve depends sensitively on the shape, sizes, and crystalline anisotropies of the device components [39,40].

In this work, we present detailed numerical analysis of magnetic field dependencies of the critical current  $I_c(H)$  and other characteristics of Josephson spin valves with different geometries and sizes. Our main motivation is to clarify how to recognize signatures of unconventional spin-triplet and long-range spin-singlet contributions to the supercurrent. The analysis is based on realistic micromagnetic simulations for Ni-based ferromagnets. In order to understand the role of magnetic domain structure, we consider monodomain, few-domain, and polydomain states for JSV's of different sizes. The characteristic size is determined by the flux quantization condition from either the coercive field or the saturation magnetization of the ferromagnet. For small devices, the induced flux is much smaller than the flux quantum  $\Phi_0$  and

for large JSV larger than  $\Phi_0$ . In small monodomain JSV's, the triplet supercurrent component is clearly manifested by a dissimilar double-maxima feature in  $I_c(H)$ . With increasing size it is, however, overshadowed by Fraunhofer oscillations of the supercurrent at the flux quantization condition. In case of multiple domains, the double maxima are smeared out and reduced in amplitude. In the polydomain case, they turn into a single broad maximum, which may be difficult to unambiguously ascribe to the triplet current in the experimental case. The only remaining signature of the triplet current in polydomain case are beatings in  $I_c(H)$  with a half-flux quantum periodicity. Since increasing of the JSV size leads both to appearance of the polydomain state and to rapid oscillations of  $I_c(H)$  due to flux quantization, it becomes difficult to identify the spin-triplet component of the supercurrent from measured  $I_c(H)$  patterns of large JSV's, without a detailed knowledge of the spin-valve state. However, we argue that the unambiguous conclusions can be made from a systematic analysis of size, thickness, and shape dependencies of the Josephson spin-valve characteristics made on the same chip in combination with *in situ* characterization of specific JSV's. This is our main advice for the future experimental work.

## II. NUMERICAL SIMULATIONS

We consider a rectangular SF<sub>1</sub>NF<sub>2</sub>S JSV with sizes  $L_x \times L_y$  in the  $xy$  plane. The spin valve consists of two dissimilar ferromagnetic layers F<sub>1,2</sub> ( $F_1 \neq F_2$ ) with thicknesses  $d_{1,2}$ , separated by a normal metal N(Cu) spacer with the thickness  $d_N$ . It is sandwiched between two superconducting layer of thickness  $d_S$  and the London penetration depth  $\lambda$ .

### A. Micromagnetic simulations

Micromagnetic simulations were performed using OOMMF software [41]. We present calculations for pure Ni and diluted CuNi F layers. In case of Ni we used standard input parameters suggested by the software: the saturation magnetization  $M_s = 4.910^5$  A/m (in CGS units  $4\pi M_s = 6158$  G), the exchange coupling constant  $A = 9 \times 10^{-12}$  J/m for Ni, the cubic crystalline anisotropy  $K_1 = -5.710^3$  J/m<sup>3</sup>, and the damping constant  $a = 0.5$ . In case of the Cu<sub>1-x</sub>Ni<sub>x</sub> alloy we scaled the relevant parameters proportional to Ni concentration  $x$ . For CuNi we also changed the exchange coupling  $A = 0.5-2 \cdot 10^{-12}$  J/m in order to tune the domain size, the smaller is  $A$ , the smaller is the domain structure.

For Ni-based JSC the dissimilarity between F layers is achieved by using different thicknesses  $d_1 = 5$  nm and  $d_2 = 7.5$  nm. The spacer thickness is  $d_N = 10$  nm. The mesh size in  $z$  direction is  $dz = 2.5$  nm and in the  $(x, y)$  plane  $dx, dy = 2-20$  nm. For CuNi-based JSV the dissimilarity was achieved by taking different Ni concentration  $x_1 = 0.5$  and  $x_2 = 0.6$ , while thicknesses were the same  $d_1 = d_2 = d_N = 10$  nm.

Our micromagnetic simulations were made solely for the F<sub>1</sub>NF<sub>2</sub> spin valve, not including possible screening effects from S layers. In the monodomain case, those effects are negligible. Therefore, simulations for the monodomain case should be quantitatively correct. However, in the polydo-

main case, S layers can affect domain sizes [42,43]. To analyze the effect of domain sizes and configuration on JSV characteristics, we tuned the exchange coupling constant  $A$  in the CuNi-based JSV. The smaller is the coupling, the smaller is the domain size. This allows us to make general qualitative conclusions in the polydomain case as well.

The output of micromagnetic simulation is spatial distribution of three components of magnetization  $M_{x,y,z}(x, y, z)$ . In all cases, we had the in-plane anisotropy of magnetization. The out-of-plane component of magnetization  $M_z \simeq 0$  and variation of the magnetization state across the layers,  $M_{x,y}(z)$ , were negligible and will not be shown. Simulations are made for varying magnetic fields  $H_x$ , applied parallel to the planes in the  $x$ -axis direction.

The sizes and the shapes of JSV's play important roles: (i) changing sizes leads to changing in the number of magnetic domains, which in turn leads to a change in magnetization curves. (ii) With increasing sizes, a larger flux penetrates into the JSV at a given field. The flux in the JSV is quantized. Size-dependent flux quantization in the JSV leads to a strong modulation of the critical current [26]. (iii) The shape of the JSV affects the shape anisotropy, which determines magnetic properties of the JSV. Below, we consider all the three aspects of size and shape variation. In order to change flux quantization conditions in the JSV we varied sizes  $L_{x,y}$ , S-layer thickness  $d_S$ , and to some extent the London penetration depth (staying within a realistic range for Nb thin films). Since variation of the size affects magnetic properties of the JSV (coercive field, domain structure, shape anisotropy), variation of  $d_S$  and  $\lambda$  allows more unambiguous analysis of the flux quantization effect alone without changing the magnetic structure of the JSV.

### B. Critical current calculation

Following Ref. [10], we assume that the Josephson current has three main components: short-range spin singlet  $I_{ss}(x, y)$ , long-range spin singlet  $I_{sl}(x, y)$ , and long-range odd-frequency spin triplet  $I_{tr}(x, y)$ . Local values of those currents depend on local values of relative angles between magnetizations of the two F layers  $\alpha(x, y)$  and the Josephson phase difference between S electrodes  $\varphi(x, y)$ :

$$I_{ss}(x, y) = I_{ss0} \cos^2[\alpha(x, y)/2] \sin[\varphi(x, y)], \quad (1)$$

$$I_{sl}(x, y) = I_{sl0} \sin^2[\alpha(x, y)/2] \sin[\varphi(x, y)], \quad (2)$$

$$I_{tr}(x, y) = I_{tr0} \sin^2[\alpha(x, y)] \sin[2\varphi(x, y)]. \quad (3)$$

We made calculations for a variety of amplitudes  $I_{ss0}$ ,  $I_{sl0}$ ,  $I_{tr0}$ , including different signs of some components. This, however, does not change qualitative conclusions, which can be deduced from inspection of separately shown singlet and triplet components. Therefore, in order to limit the number of variables, we only present calculations for one set of the amplitudes:  $I_{ss0} = 0.1$ ,  $I_{sl0} = 1.0$ ,  $I_{tr0} = 3.0$ .

We assume that JSV's are in the short junction limit, i.e., sizes  $L_x, L_y$  are smaller than the Josephson penetration depth.

In this case,

$$\frac{\partial \varphi(x, y)}{\partial y} = \frac{2\pi \Lambda}{\Phi_0} H_x + \frac{2\pi d_1}{\Phi_0} 4\pi M_{x1} + \frac{2\pi d_2}{\Phi_0} 4\pi M_{x2}, \quad (4)$$

$$\frac{\partial \varphi(x, y)}{\partial x} = \frac{2\pi d_1}{\Phi_0} 4\pi M_{y1} + \frac{2\pi d_2}{\Phi_0} 4\pi M_{y2}. \quad (5)$$

Here,  $H_x$  is the applied magnetic field in the  $x$ -axis direction,  $M_{x1}(x, y)$ ,  $M_{x2}(x, y)$ ,  $M_{y1}(x, y)$ , and  $M_{y2}(x, y)$  are local values of  $M_x$  and  $M_y$  magnetization components in  $F_1$  and  $F_2$  layers, respectively, obtained from micromagnetic calculations and

$$\Lambda = d_1 + d_2 + d_N + 2\lambda \tanh(d_S/2\lambda) \quad (6)$$

is the magnetic thickness of a Josephson junction. The Josephson phase distribution is calculated by direct integration of Eqs. (4) and (5) starting from one of the corners of the JSV. To minimize the numerical error, we used an averaged value of the phase integrated from the four corners of the JSV.

The  $x, y$  components of the total flux through the JSV

$$\Phi_x = L_y[\Lambda H_x + d_1 4\pi M_{x1} + d_2 4\pi M_{x2}], \quad (7)$$

$$\Phi_y = L_x[d_1 4\pi M_{y1} + d_2 4\pi M_{y2}] \quad (8)$$

are increasing with the size and layer thicknesses.

The net supercurrent  $I_s = I_{ss} + I_{sl} + I_{tr}$  [Eqs. (1)–(3)] is integrated over the JSV area using the obtained values  $\alpha(x, y)$  and  $\varphi(x, y)$ . To find the critical current (both positive and negative values), we maximized the supercurrent with respect to the arbitrary phase offset  $\varphi_0$ ,  $\varphi(x, y) = \varphi_0 + \varphi(x, y)$ .

### III. RESULTS

#### A. Monodomain case

We start our analysis with the simplest case of the monodomain state of the spin valve. Figure 1 represents calculations made for small square-shape Ni(5 nm)/Cu(10 nm)/Ni(7.5 nm) spin valves with different sizes  $L_x = L_y = 30, 50,$  and 100 nm. Figure 1(a) shows magnetization loops  $M_x(H_x)$ . The magnetization states for the three square JSV's are essentially identical (size independent for the same shape). All of them are in the monodomain state.

Figure 1(b) represents magnetization distributions in the two F layers for the  $100 \times 100$  nm<sup>2</sup> JSV at points A–F for the downward sweep from positive to negative field, marked in Fig. 1(a) (note that colors represent only the  $y$  component of magnetization). It can be seen that the spin valve is in a “scissor” state when magnetizations of the two F layers gradually rotate in opposite directions with decreasing field. At point C, the  $M_x$  component in the thinner  $F_1$  layer flips and the spin valve switches into a magnetostatically stable antiparallel (AP) state. Here, the magnetization is oriented along one of diagonals due to the shape anisotropy. The stable AP state is manifested by a pronounced step C–D in the magnetization curve [26]. With further increase of (negative) field the moment of the thicker  $F_2$  layer also flips and the spin valve gradually approaches the parallel state in the scissor manner (see points E and F).

Figure 1(c) shows  $M_y$  components of magnetization for the downward field sweep. The maximum of  $|M_y|$  is achieved at the end of the AP step, point D. Note that the magnetization

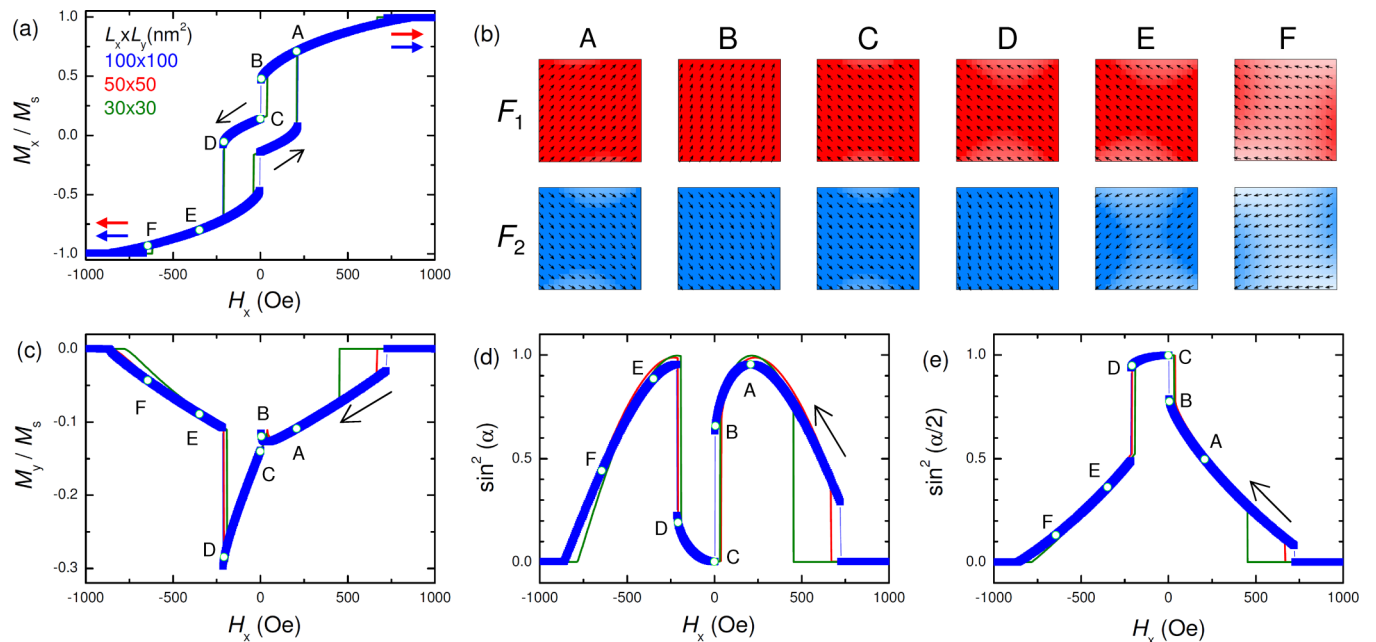


FIG. 1. Characteristics of a monodomain “scissor” switching of square-shape spin valves Ni(5nm)/Cu(10nm)/Ni(7.5nm) of different sizes. (a) Calculated magnetization loop  $M_x(H_x)$ . Note pronounced intermediate step CD, which manifests the magnetostatically stable antiparallel state of the spin valve. (b) Configuration of magnetization of the two ferromagnetic layers  $F_{1,2}$  at points A–F along the magnetization curve. A monodomain scissorlike rotation of magnetization can be seen. (c) Perpendicular to the field magnetization  $M_y(H_x)$  for a downward field sweep. (d), (e) Show average values of  $\sin^2$  of the angle and half the angle between local magnetizations in the two F layers. They represent relative amplitudes of the triplet (d) and the long-range singlet (e) supercurrents, respectively. Note appearance of the characteristic dissimilar double maxima of the triplet current (d) on both sides of the AP state CD.

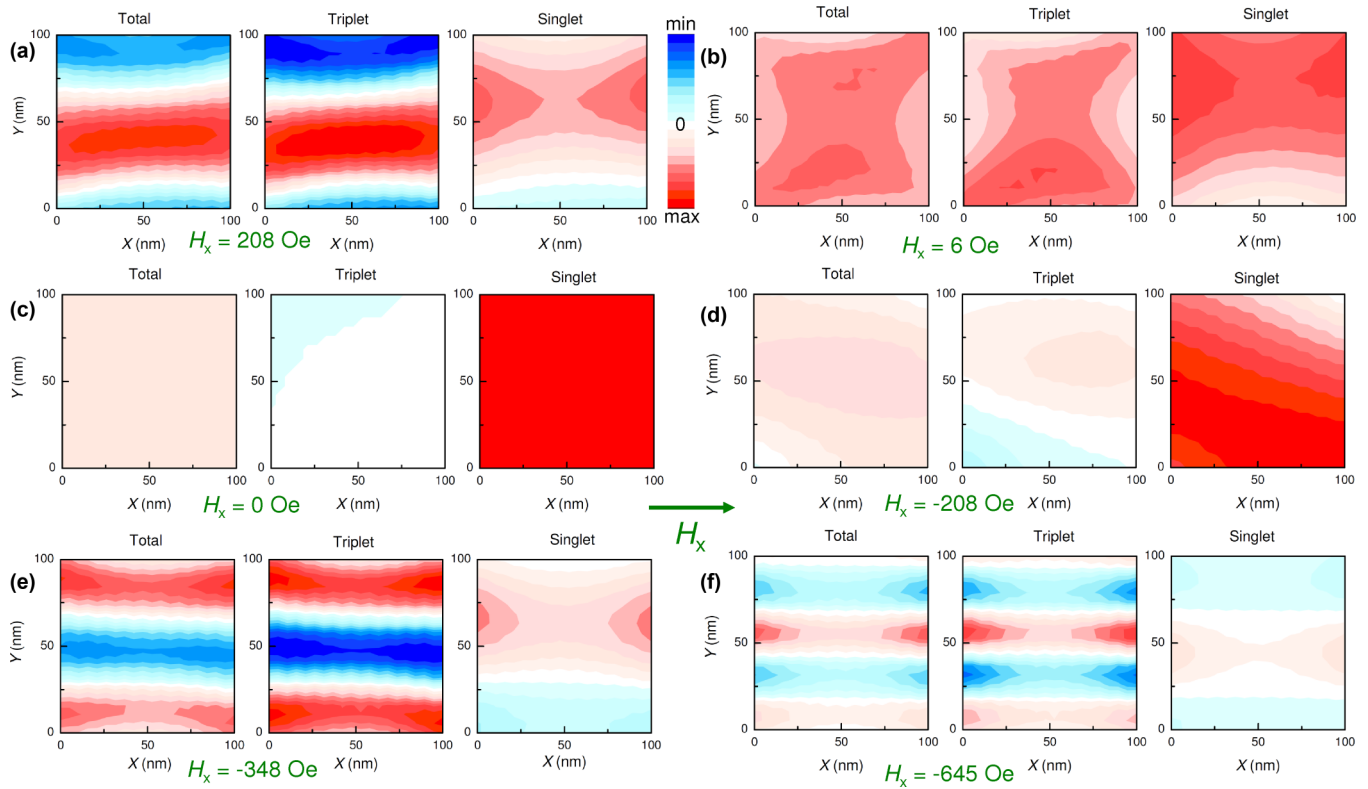


FIG. 2. Spatial distribution of supercurrents in a monodomain JSV  $100 \times 100 \text{ nm}^2$  at points A–F, marked in Fig. 1(a), at maximal positive currents. Left, middle, and right panels represent total, triplet, and singlet currents, respectively. Sign-reversal oscillations at high fields (points A, E, F) are due to flux quantization. Note that the triplet current oscillates with a factor 2 shorter period than the singlet due to the double-harmonic current-phase relation.

orientation continues to change even at the AP step (compare points C and D).

Figures 1(d) and 1(e) represent spatially averaged values of  $\sin^2(\alpha)$  and  $\sin^2(\alpha/2)$ , respectively, for the downward field sweep. They represent relative amplitudes of Fig. 1(d) the triplet and Fig. 1(e) the long-range singlet components of the supercurrent [see Eqs. (2) and (3)]. The most noncollinear state with  $\alpha = \pi/2$  and maximum of the triplet current is achieved at point A, while at point C it is in the pure AP state  $\alpha = \pi$ , at which there is large long-range singlet, but no triplet current. The noncollinear state is restored again after switching from the AP state, point E. Thus, for every field sweep there are two dissimilar maxima of the triplet current at both sides of the AP state. This double maxima is the most characteristic signature of the triplet current, which can be used for its identification.

The long-range singlet current [Fig. 1(e)] has a single maximum at the AP step. Note that it has the same functional dependence as the perpendicular (tunneling) magnetoresistance or the spin valve [44], which can be used for comparison with experiment [26].

Figure 2 represents color maps of the spatial distribution of the total (left), triplet (middle), and singlet (right panel) supercurrents in the  $100 \times 100 \text{ nm}^2$  JSV at the same points A–F. Simulations are done for Nb(250 nm) Ni(5 nm)/Cu(10 nm)/Ni(7.5 nm) Nb(250 nm) JSV with  $\lambda = 150 \text{ nm}$  and the magnetic thickness  $\Lambda = 227 \text{ nm}$  [see Eq. (6)]. Those current distributions correspond to the positive critical current  $I = I_c$  at the corresponding fields.

At low fields, when the flux produced by the field and the magnetization inside the JSV is significantly lower than  $\Phi_0$ , current components are governed by the orientation of magnetizations  $\alpha$  [see Figs. 1(d) and 1(e)]. For example, in the noncollinear state B the triplet current is large, but in the AP state at point C it is very small and almost all of the current is singlet. At higher fields, however, the effect of flux quantization becomes important. It is seen that at high fields (points E and F) currents start to oscillate along the  $y$  direction. This is a consequence of flux quantization in the applied field  $H_x$  and the internal magnetization  $M_x$ . Such oscillations have a profound effect and greatly reduce the critical current. For example, at point E there is almost a full amplitude of the triplet current, but the net supercurrent remains very small because positive and negative currents cancel each other. Note that the triplet current has a two-times shorter oscillation period than the singlet current because  $I_{tr}$  has a double-harmonic current-phase relation [Eq. (3)].

Figures 3(a)–3(c) show magnetic field dependencies of the critical current [Fig. 3(a)] and the corresponding triplet [Fig. 3(b)], and singlet [Fig. 3(c)] components for a small square-shaped JSV  $50 \times 50 \text{ nm}^2$  with monodomain scissor state see (Fig. 1). Here, we only show the downward sweep from positive to negative field. Calculations are done for thin S electrodes with  $d_S = 50 \text{ nm}$  and  $\lambda = 150 \text{ nm}$ , leading to a small  $\Lambda = 72 \text{ nm}$ . A combination of small  $L_y$  and  $\Lambda$  leads to a small flux in the JSV [Eqs. (7) and (8)]. In this case, flux quantization is not important,  $\Phi_{x,y} < \Phi_0$ , and singlet

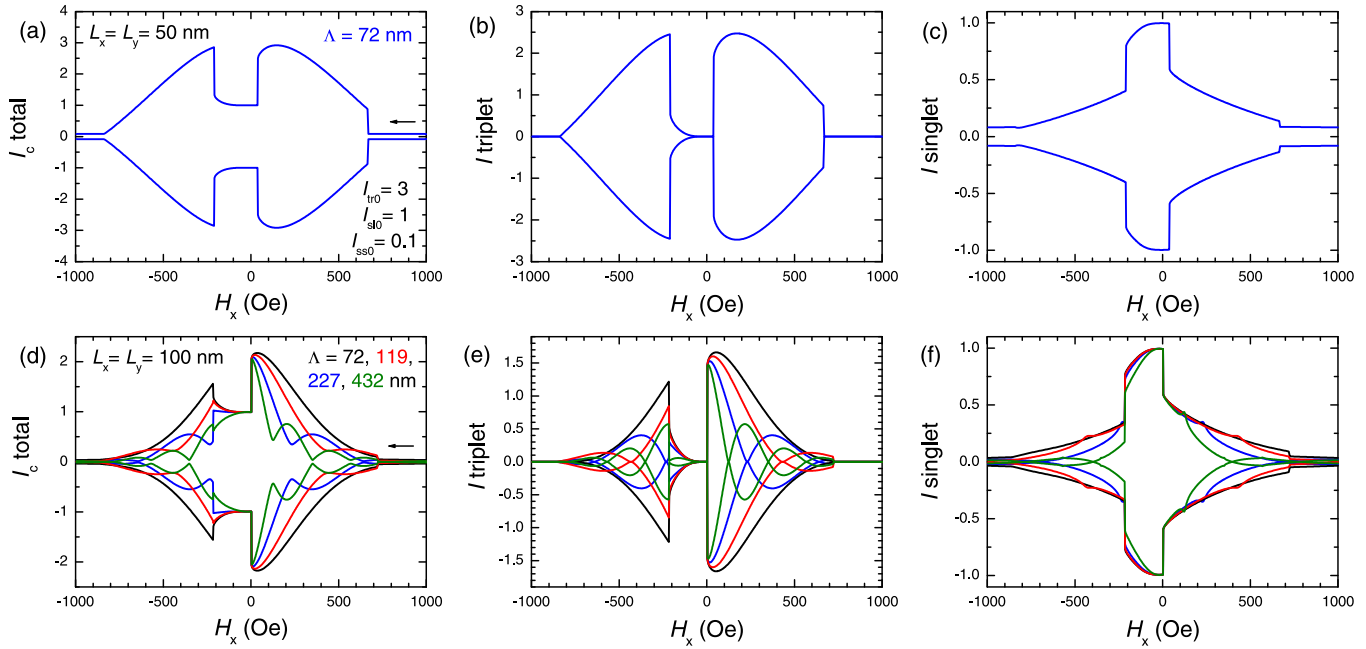


FIG. 3. Field dependencies of positive and negative critical currents for monodomain square-shape JSV's with different sizes (for a downward field sweep only). Left, middle, and right panels represent total, triplet, and singlet currents, respectively. (a)–(c) For a small  $50 \times 50 \text{ nm}^2$  and thin-layer JSV in which flux quantization is negligible. Here, a characteristic dissimilar double maximum is seen, which follows the corresponding feature in the triplet current amplitude  $I_{tr} \propto \sin^2(\alpha)$ , Fig. 1(d). (d)–(f) Show systematic distortion of the double maximum in the larger  $100 \times 100 \text{ nm}^2$  JSV upon increasing of the magnetic thickness  $\Lambda$  due to flux-quantization effect. For the largest  $\Lambda = 432 \text{ nm}$  the second maximum in  $I_c(H)$  is completely removed.

and triplet current components are simply determined by the relative magnetization angle  $\alpha$ ,  $I_{\text{triplet}} \simeq I_{tr0} \sin^2(\alpha)$ ,  $I_{\text{singlet}} \simeq I_{sl0} \sin^2(\alpha/2)$  as seen from comparison with Figs. 1(d) and 1(e). The triplet current is manifested by a dissimilar double maximum on both sides of the AP state. It is quite characteristic and should be easily recognizable in experiment.

However, flux quantization may strongly distort such a simple picture. Figures 3(d)–3(f) demonstrate the effect of flux quantization in the applied magnetic field  $H_x$ . The flux at a given field can be increased either by increasing the size of the JSV, or the magnetic thickness  $\Lambda$  [Eq. (6)]. The latter can be easily tuned by changing the S-layer thickness and by using temperature dependence of  $\lambda$ . Changing  $L_{x,y}$  and  $\Lambda$  are equivalent, except that some details of the magnetic state do depend on the size due to edge effects: even in the monodomain case, shown in Fig. 1, there are some size-dependent variations. Therefore, in order to completely exclude such variations, in Figs. 3(d)–3(f) we change flux quantization conditions solely by changing  $\Lambda$  while keeping the magnetic state exactly the same, corresponding to the  $100 \times 100 \text{ nm}^2$  Ni(5 nm)/Cu(10 nm)/Ni(7.5 nm) spin valve, shown in Fig. 1. Flux quantization leads to sign-reversal circulation of current (see point F in Fig. 2), resulting in suppression of the net supercurrent. Since singlet and triplet components have single- and double-harmonic current-phase relations [see Eqs. (1)–(3)], the triplet current is oscillating with a two-times shorter period both in space along the  $y$ -axis (refer to central and right panels in Fig. 2 F) and field [refer to Figs. 3(e) and 3(f)].

From Fig. 3(d) it is seen that for the small  $\Lambda = 72 \text{ nm}$  (black lines) the triplet double maximum is still recognizable, even though the amplitude of the second maximum is reduced approximately twice with respect to the smaller JSV [shown in Fig. 3(a)] due to a finite flux at the corresponding field  $H_x \simeq -250 \text{ Oe}$ . With increasing  $\Lambda$  the flux increases as the second maximum progressively decreases. For the largest  $\Lambda = 432 \text{ nm}$  (olive curves), it becomes practically indistinguishable in the total  $I_c(H)$ . The amplitude of the first maximum is affected marginally because it occurs close to zero field and corresponds to a small flux.

From Fig. 3 it is seen that the characteristic signature of the triplet current, the double maximum in  $I_c(H)$ , is washed away by flux quantization effects. In particular, the second maximum of the triplet current is washed away for junctions wider than  $L_y^* = \Phi_0/2H_{AP}\Lambda \simeq 180 \text{ nm}$ , where  $H_{AP} \simeq 250 \text{ Oe}$  is the field of switching from the AP state [see point D in Fig. 1(a)] and  $\Lambda = 227 \text{ nm}$  ( $d_S = 250 \text{ nm}$ ,  $\lambda = 150 \text{ nm}$ ). The factor  $\Phi_0/2$  is due to the double-harmonic dependence  $I_{tr}(\varphi)$ . A similar suppression occurs in long JSV  $L_x^* \gtrsim 560 \text{ nm}$  due to finite value of the  $M_y$  component  $\Phi_y(H_{AP}) > \Phi_0/2$ . Simultaneously the maximum achievable critical current density is rapidly decreasing with increasing  $L_{x,y}$  and/or  $\Lambda$ . For larger JSV's  $L_{x,y} \gtrsim L_{x,y}^*$  the triplet double maxima is washed away and the triplet component can no longer be unambiguously identified from the  $I_c(H_x)$  pattern without detailed knowledge of the spin-valve state even for the simplest monodomain case. However, as follows from Fig. 3(d), a systematic analysis of thickness and size dependencies of  $I_c(H)$  for JSV's of different

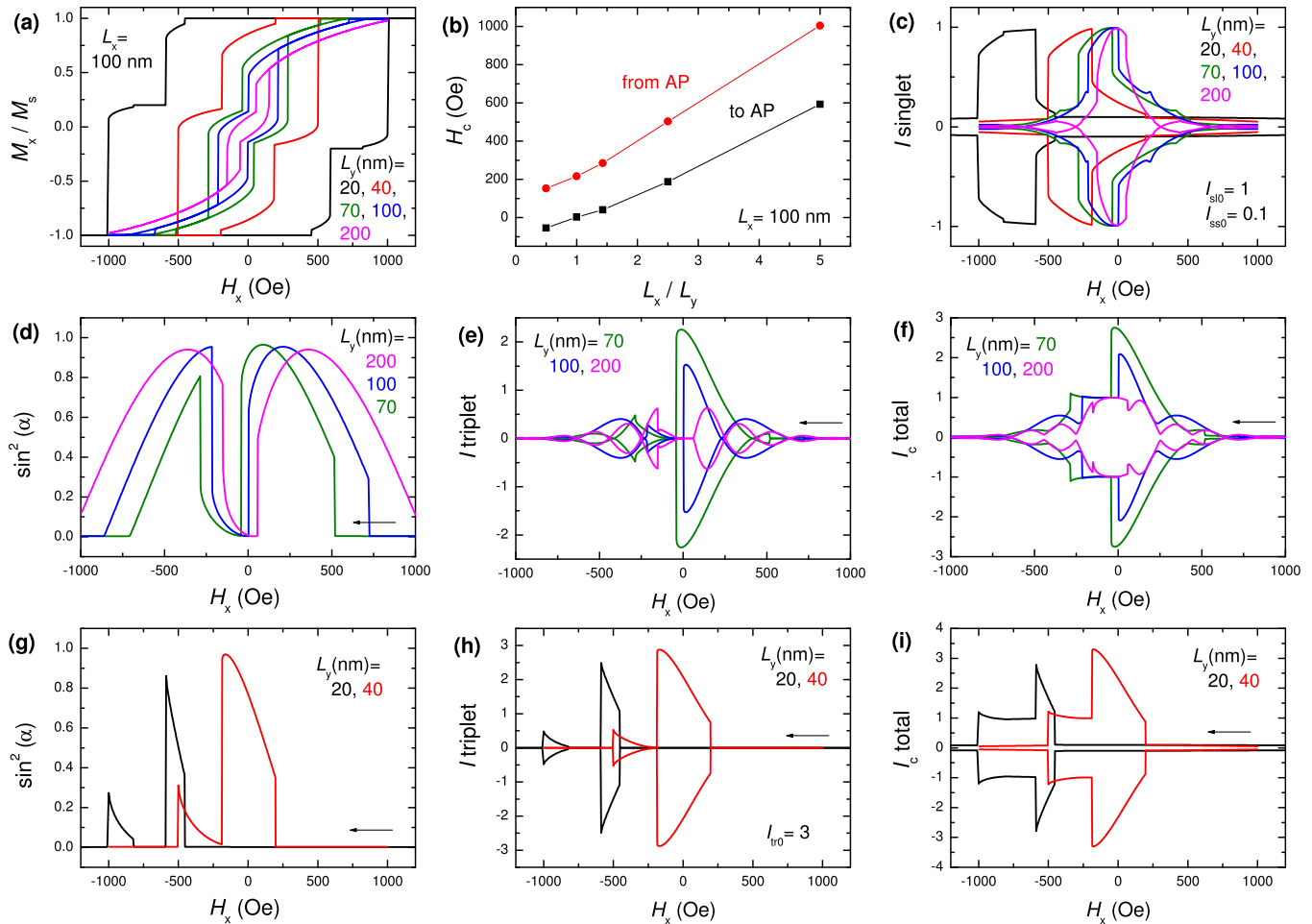


FIG. 4. Field dependencies of characteristics of rectangular monodomain JSV's with  $L_x = 100$  nm and different  $L_y$ . (a) Magnetization loops  $M_x(H_x)$ . It is seen that switching fields to and from the AP state depends on the shape. (b) Field values for switching into (black) and from (red) the antiparallel state as a function of the aspect ratio  $L_x/L_y$ . (c) Field dependence of the singlet contribution to the critical current (for a downward field sweep only). The pronounced maximum occurs in the AP state and is due to the long-range singlet current. (d)–(f) Field dependence of characteristics of JSV's with not very large aspect ratios: (d) the average  $\sin^2(\alpha)$ , (e) the triplet contribution to the critical current, and (f) the total critical current. For the largest JSV  $L_y = 200$  nm flux quantization effect smears out both triplet maxima in  $I_c(H)$ , despite it is very pronounced in  $\sin^2(\alpha)$  [magenta line in (d)]. (g)–(i) Field dependence of characteristics of JSV's with large aspect ratios. (g) The average  $\sin^2(\alpha)$ . It is seen that for elongated JSV  $L_y = 20$  nm (black line) the increasing shape anisotropy starts to suppress the range of existence of the noncollinear state, especially the second maximum. (h) The triplet contribution to the critical current. (i) The total critical current. Here, the double maximum is removed by the strong shape anisotropy.

sizes at the same chip can still provide a clue about the triplet component. Such an analysis requires, however, that the magnetic state of those JSV's is size independent.

In Fig. 1 we demonstrated that magnetic states of spin valves may indeed be size independent under certain conditions. First of all, we emphasize that the size independence occurs only for spin valves *with the same shape* and only within a certain range of sizes. Magnetic properties of ferromagnetic nanoparticles are determined by their demagnetization factors, which determine the shape anisotropy [45,46]. For particles with the same shape (squares considered above) the demagnetization factor is weakly dependent on size, provided it is significantly larger than the thickness,  $L_x = L_y \gg d_{1,2}$ . For  $d_{1,2}$  of 5 and 7.5 nm, size independence holds down to approximately  $L_{x,y} \simeq 30$  nm. Smaller JSV's  $L_{x,y} = 20$  nm have different coercive fields [see Fig. 4(a)] because they are

no longer flat and have significantly different demagnetization factors than thin films. The upper limit is determined by the domain size, which however is not a universal number, but also depends on the shape of the particle (typically several hundreds of nm for Ni).

## B. Shape dependence of the magnetic state

The magnetic state of ferromagnetic nanoparticles depends on their demagnetization factors, which define the shape anisotropy [45,46]. This makes the shape an additional variable in the JSV dynamics.

In Fig. 4(a) we show calculated magnetization loops  $M_x(H_x)$  for rectangular Ni(5 nm)/Cu(10 nm)/Ni(7.5 nm) spin valves with fixed  $L_x = 100$  nm, but different  $L_y$  from 20 to 200 nm. In all cases, spin valves are in the monodomain

scissor state. However, it is seen that the fields for switching to and from the AP state are largely different. In Fig. 4(b) we plot corresponding switching fields to (black) and from (red) the AP state. It is seen that both vary quasilinearly with the aspect ratio  $L_x/L_y$ . Thus, the AP state, corresponding to the minimum of the triplet and maximum of the singlet current is shifted to larger fields with increasing the aspect ratio, as shown in Fig. 4(c).

In Figs. 4(d)–4(f) we analyze the influence of the shape on JSV characteristics for not very large aspect ratios. Figure 4(d) shows the spatially average of  $\sin^2(\alpha)$ , which represents the amplitude of the triplet current, Eq. (3). For  $L_y = 200$  nm (magenta curves) the field is applied along the short, hard axis. This leads to an almost uniform scissorlike rotation of the moments in the two F layers, leading to asymmetric, but equal amplitude double maxima. With increasing the aspect ratio, the asymmetry increases. Already in a slightly elongated

JSV with  $L_y = 70$  nm (olive curves), the second maximum after switching from the AP state becomes significantly lower than the first maximum before switching into the AP state. The asymmetry is caused by increasing stability of the AP state in case when the field is applied along the easy axis of magnetization.

In Figs. 4(g)–4(i) we show a similar analysis for elongated JSV's with large aspect ratios. From Fig. 4(g) it is seen that the asymmetry of the double maximum in  $\sin^2(\alpha)$  is further progressing with increasing the aspect ratio. For the most elongated JSV with  $L_y = 20$  nm, even the first maximum is reduced. In this case, the strong shape anisotropy tries to keep magnetization in the collinear (parallel or antiparallel) state, reducing the range of the noncollinear magnetization with nonzero  $\sin^2(\alpha)$ . Thus, a strong shape anisotropy (for field along the easy axis) is detrimental for generation of the triplet current.

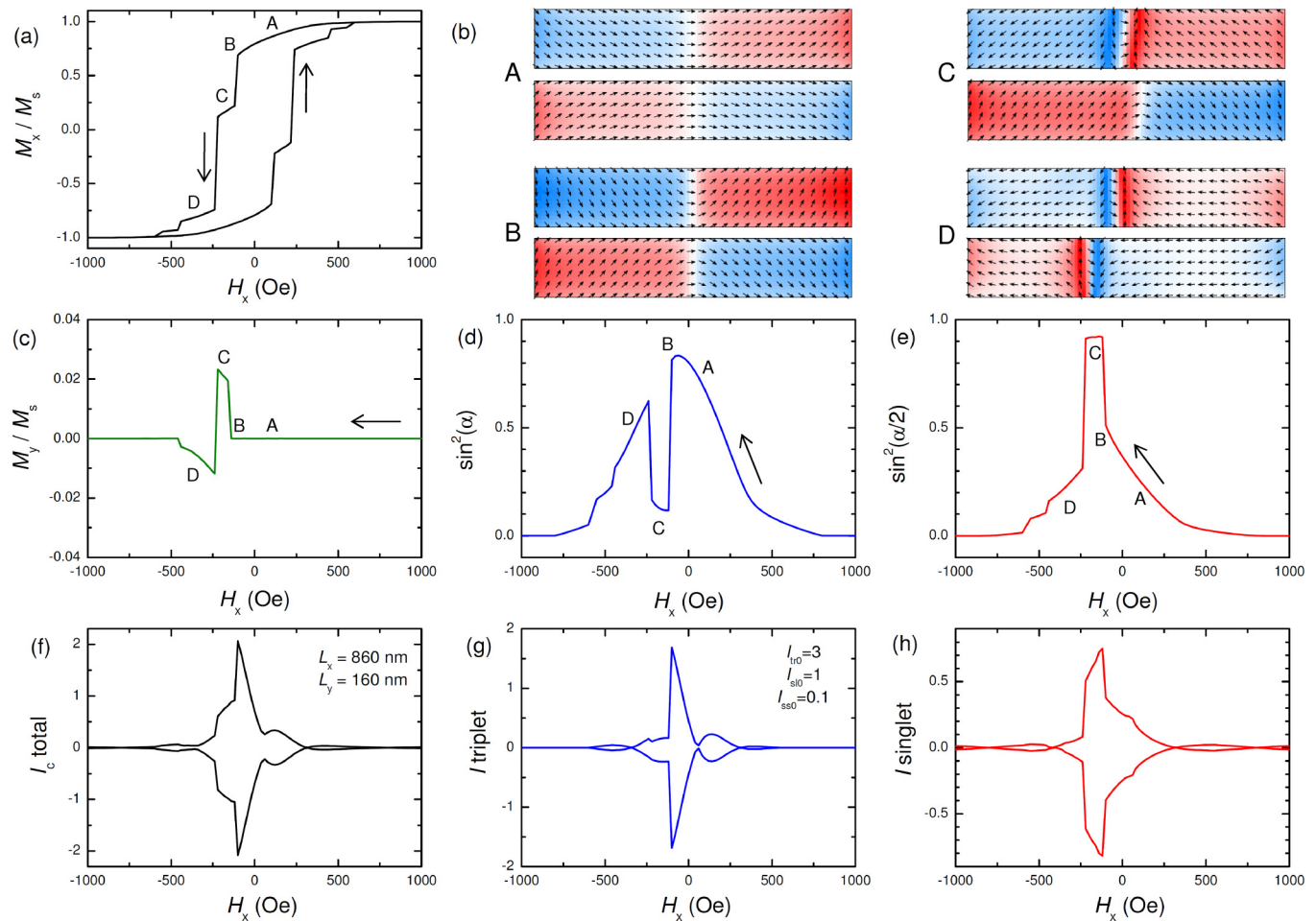


FIG. 5. Characteristics of a two-domain switching of a spin-valve Ni(5 nm)/Cu(10 nm)/Ni(7.5 nm) with an elongated rectangular shape  $860 \times 160$  nm<sup>2</sup>. (a) Calculated magnetization loop  $M_x(H_x)$ . Four jumps correspond to sequential switching between monodomain and two-domain states. The pronounced intermediate step C corresponds to the predominantly antiparallel state of the spin valve. (b) Configuration of magnetization of the two ferromagnetic layers  $F_{1,2}$  at points A–D along the magnetization curve. Note that the spin-valve configuration at point C with two domains in  $F_1$  and a monodomain “C” state in  $F_2$  is locally almost antiparallel. (c) Perpendicular to the field magnetization  $M_y(H_x)$  for a downward field sweep. Note that appearance of domains greatly reduces  $M_y$  compared to the monodomain scissors state [Fig. 1(c)]. (d), (e) Show average values of  $\sin^2$  of the angle and half of the angle between local magnetizations in the two F layers. Note that the double maximum in  $I_{tr0}$  (d) is still clearly seen, but it has reduced amplitude compared to the monodomain case [Fig. 1(d)]. (f)–(h) Field dependencies of the total critical current (f), the triplet (g), and the singlet (h) contributions. It is seen how the triplet double maximum is completely removed.

Figures 4(e) and 4(h) show corresponding size and shape dependencies of magnetic field modulations of the maximum triplet current. For narrow JSV's [Fig. 4(h)], flux quantization is not important and  $I_{tr}(H_x)$  is determined by  $\sin^2(\alpha)$ . For larger  $L_y$  [Fig. 4(e)], flux quantization starts to play the role and tends to suppress the double maxima, similar to that in Fig. 3(d).

Figures 4(f) and 4(i) show size and shape dependencies of  $I_c(H)$  modulation patterns. Note that in all cases the double maximum is not visible, although for different reasons. For narrow JSV's [Fig. 4(i)], the second maximum is suppressed by the strong shape anisotropy that suppresses the noncollinear state after switching from the AP state. For broader JSV's, maxima are suppressed by flux quantization. For the broadest JSV,  $L_y = 200$  nm, both maxima are suppressed by flux quantization, despite profound maxima in  $\sin^2(\alpha)$  [see Fig. 4(d)].

We emphasize that according to Figs. 3(d) and 4(f) and 4(i) dramatic variations of  $I_c(H)$  patterns for relatively small changes of sizes and shapes occur even in case of the simplest monodomain state of the JSV.

### C. Two-domain case

Next, we consider the case with two domains (one domain wall) per F layer. For Ni(5 nm)/Cu(10nm)/Ni(7.5 nm) spin valves, such state is realized in elongated valves  $L_x > L_y$  in a broad range of sizes from slightly more than 100 nm to almost a  $\mu\text{m}$ . Figure 5 shows results for a  $860 \times 160$  nm<sup>2</sup> JSV. Figure 5(a) shows the magnetization loop  $M_x(H_x)$ . Figure 5(b) shows magnetization orientations at points A, B, C, D at the downward field sweep, marked in Fig. 5(a). It is seen that upon decreasing field (points A and B) magnetization configuration in both F layers acquires a "C" shape. After point B the thinner  $F_1$  (top) layer switches into the two-domain state. This leads to establishing of the antiparallel orientations of the JSV on both sides of the domain wall (point C). After that, the thicker  $F_2$  layer switches into the two-domain state (point D), then  $F_1$  and  $F_2$  sequentially switch back into the "C" state. This switching leads to appearance of four jumps in  $M_x(H_x)$  curve [Fig. 5(a)] instead of the one AP step in the monodomain case [Figs. 1(a) and 4(a)].

Figures 5(d) and 5(e) show average  $\sin^2(\alpha)$  and  $\sin^2(\alpha/2)$ , representing amplitudes of the triplet and the long-range singlet components of the supercurrent, respectively. From comparison of Figs. 5 and 1 it is seen that the single-domain wall does not change the qualitative behavior of the triplet [Fig. 5(d)] and the long-range singlet [Fig. 5(e)] components. However, it does reduce the overall modulation of the double maxima in the amplitude of the triplet component  $\propto \sin^2(\alpha)$ . Both the first maximum (B) and especially the second (D) are significantly less than 1 and the minimum (C) is larger than 0. Thus, the single-domain wall smears out but does not completely remove the triplet current modulation.

In Figs. 5(f)–5(h) we show magnetic field dependencies of the total critical currents [Fig. 5(f)] and the corresponding triplet [Fig. 5(g)] and singlet [Fig. 5(h)] components. The general behavior is similar to that in the monodomain case. From the shape of  $I_c(H_x)$  in Fig. 5(f) it is difficult to guess about the underlying double maximum in the triplet current amplitude [Fig. 5(d)].

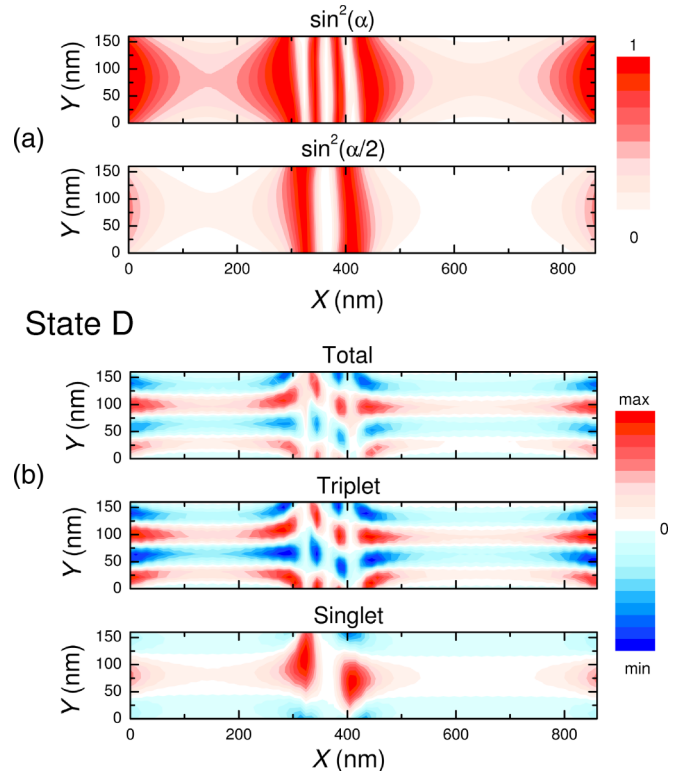


FIG. 6. Color maps of spatial distributions of (a)  $\sin^2(\alpha)$  and  $\sin^2(\alpha/2)$  and (b) maximum total, triplet, and singlet currents for the  $860 \times 160$  nm<sup>2</sup> JSV at point D [see Fig. 5(a)]. It is seen how the domain walls intermix singlet and triplet components.

Figure 6 shows color maps of spatial distributions of (a)  $\sin^2(\alpha)$  and  $\sin^2(\alpha/2)$  and (b) maximum total, triplet, and singlet currents for the  $860 \times 160$  nm<sup>2</sup> JSV at point D [see Fig. 5(a)]. From Fig. 6(a) it is seen that rotation of magnetization direction near the domain walls generates (mixes) both triplet and singlet components and, thus, smears the characteristic triplet double maximum [see Fig. 5(d)]. It also reduces amplitudes of both triplet and singlet currents. As seen from Figs. 5(d) and 5(e), maxima of  $\sin^2(\alpha)$  and  $\sin^2(\alpha/2)$  do not reach unity, unlike in the monodomain case [Fig. 1(d)]. Oscillations of currents along the vertical direction in Fig. 6(b) is due to flux quantization. The flux is close to flux quantum,  $\Phi_x \simeq \Phi_0$ , and even though the triplet current has a large amplitude, the oscillations almost cancel the total current.

### D. Polydomain case

The polydomain case occurs in larger than the domain-size spin valves. In order to get into the polydomain case we can either increase the spin-valve size or decrease the domain size. To study the polydomain case, we consider  $\text{Cu}_{1-x}\text{Ni}_x$  alloy instead of pure Ni. CuNi films with small exchange field are characterized by small domains (in our case they are in-plane oriented). We consider a rectangular-shaped spin valve  $\text{Cu}_{0.5}\text{Ni}_{0.5}(10 \text{ nm})/\text{Cu}(10 \text{ nm})/\text{Cu}_{0.4}\text{Ni}_{0.6}(10 \text{ nm})$ . The  $F_1$  and  $F_2$  layers have the same thickness, but different Ni concentration, leading to the required dissimilarity for generation of the triplet current. The domain structure in the

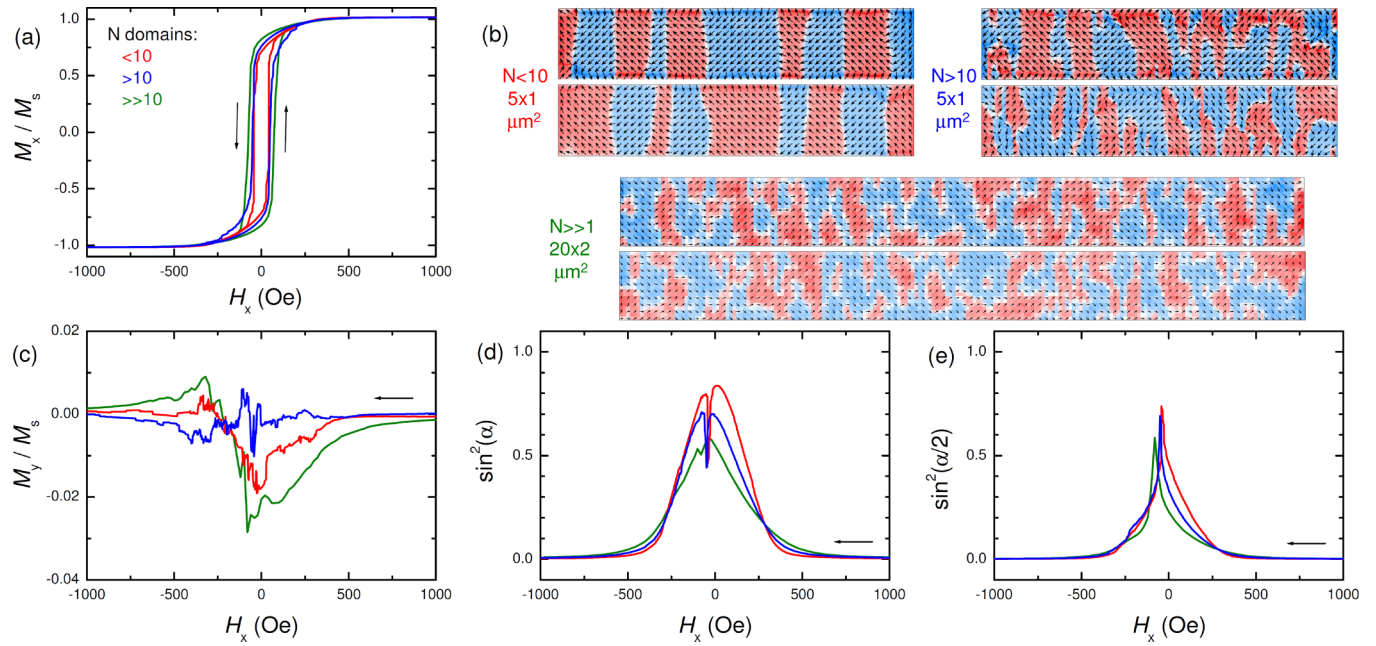


FIG. 7. Characteristics of a polydomain switching of a spin-valve  $\text{Cu}_{0.5}\text{Ni}_{0.5}(10\text{ nm})/\text{Cu}(10\text{ nm})/\text{Cu}_{0.4}\text{Ni}_{0.6}(10\text{ nm})$  with an elongated rectangular shape. (a) Calculated magnetization loop  $M_x(H_x)$ . Red and blue lines correspond  $5 \times 1 \mu\text{m}^2$  JSV's with different number of domains  $N < 10$  and  $N > 10$ . Olive line is for  $20 \times 2 \mu\text{m}^2$  JSV's with  $N \gg 10$ . Note that the intermediate AP step disappears in the polydomain case. (b) Configuration of magnetization of the two ferromagnetic layers  $F_{1,2}$  close to the remanent state for the same JSV's. (c) Perpendicular to the field magnetization  $M_y(H_x)$  for a downward field sweep. (d), (e) Show average values of  $\sin^2$  of the angle and half of the angle between local magnetizations in the two F layers. Note that the double maximum in triplet current amplitude (d) is washed away with increasing the domain number.

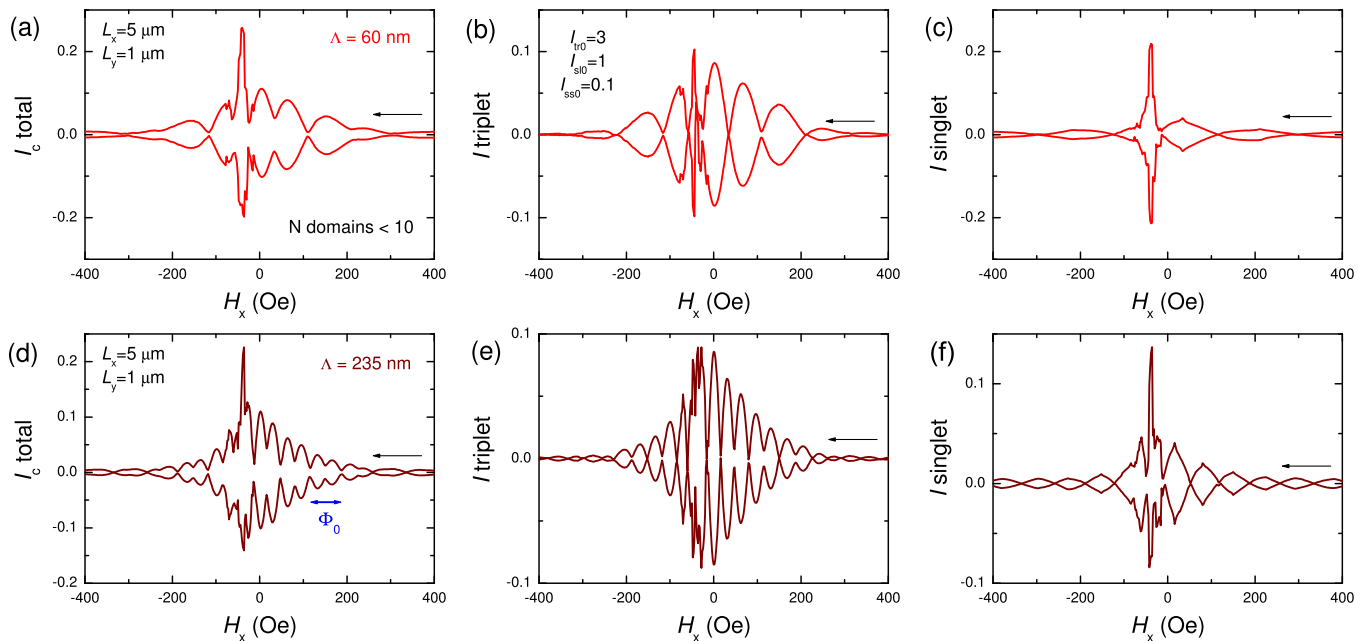


FIG. 8. Field dependencies of critical currents and their triplet and singlet components for the polydomain ( $N < 10$ ) JSV's  $5 \times 1 \mu\text{m}^2$  (for a downward field sweep). Calculations are presented for two magnetic thicknesses (a)–(c)  $\Lambda \simeq 60\text{ nm}$  and (d)–(f)  $235\text{ nm}$ . It is seen that the flux quantization effect in large polydomain JSV's makes the triplet double maximum unrecognizable. The only signature of the triplet current is seen in half-flux quantum modulation and in beatings of  $I_c(H)$  when every second minimum does not reach zero. This is due to the double-harmonic current-phase relation of the triplet current.

spin valve depends also on the exchange coupling in the F layers. The lower is the coupling, the smaller is the domain size. We tuned the exchange coupling to change the number of domains in the JSV with a given size.

Figure 7 represents corresponding calculations for three JSV's with different number of domains:  $5 \times 1 \mu\text{m}^2$  with  $N < 10$  domains (red),  $5 \times 1 \mu\text{m}^2$  with  $N > 10$  domains (blue), and  $20 \times 2 \mu\text{m}^2$  with  $N \gg 10$  domains (olive curves). Figures 7(a) and 7(c) show corresponding magnetization curves  $M_x(H_x)$  and  $M_y(H_x)$ . In the polydomain case, the  $M_y$  component becomes very small due to mutual cancellation of stray fields from domains [cf. Figs. 1(c) and 7(c)]. All  $M_x(H_x)$  loops are fairly similar. Contrary to the monodomain case, in the polydomain case there is no intermediate AP step in  $M_x(H_x)$  [47]. This can be used for distinction of the two cases [26]. Figure 7(b) shows typical domain structure (magnetization orientations) for those JSV's close to the remanent state.

Figures 7(d) and 7(e) show average  $\sin^2(\alpha)$  and  $\sin^2(\alpha/2)$ . From comparison with monodomain and two-domain data in Figs. 1 and 5(d) and 5(e) it follows that with increasing the number of domains, the characteristic double maximum of the triplet current is rapidly washed away and is replaced by a single shallow maximum with a progressively decreasing amplitude.

Figure 8 shows calculated field dependencies of supercurrents for the  $5 \times 1 \mu\text{m}^2$  JSV with the moderate number of domains  $N < 10$  for different magnetic thicknesses (a)  $\Lambda \simeq 60 \text{ nm}$  ( $d_S = 30 \text{ nm}$ ,  $\lambda = 100 \text{ nm}$ ) and (b)  $\Lambda \simeq 235 \text{ nm}$  ( $d_S = 250 \text{ nm}$ ,  $\lambda = 150 \text{ nm}$ ). It is seen that in both cases there is just one central maximum, which is impossible to *a priori* ascribe to any specific supercurrent component. As a matter of fact, those patterns are hardly distinguishable from characteristics of SFS junctions without triplet supercurrent [35]. We observed that  $I_c(H)$  patterns in the polydomain case become extremely complicated (chaotic) if domains generate more than  $\Phi_0/2$ , which precludes any sensible analysis.

## IV. DISCUSSION

### A. Mirror symmetry of $I_c(H)$ patterns in the monodomain case

From Figs. 3 and 4 it is seen that although  $I_c(H)$  patterns of JSV's can be arbitrarily different from the standard Fraunhofer modulation, in the monodomain case they always are mirror symmetric with respect to the  $H$  axis: absolute values of critical current in positive  $I_c^+$  and negative  $I_c^-$  directions are similar,  $I_c^+(H) = -I_c^-(H)$ . Such a mirror symmetry allows a clear distinction from  $I_c(H)$  distortion caused by inhomogeneity of the device. As discussed in Ref. [48], any type of spatial inhomogeneity (e.g., spatial distribution of the critical current or bias current) must preserve the central symmetry  $I_c^+(H) = -I_c^-(-H)$ . This is a consequence of space-time symmetry: simultaneous flipping of field (space) and current (time) directions is equivalent to flipping of the observer, which should not affect the result of measurements. We emphasize that our calculations are made for perfectly uniform JSV's. The mirror symmetry of  $I_c(H)$  in JSV is the result of breaking of space symmetry due to magnetic order in F layers.

The mirror symmetry is inherent only in the spatially uniform monodomain case. It leads to the uniform distribution of the bias current and precludes the self-field effect. As a result, the critical current does not depend on the direction  $I_c^+(H) = -I_c^-(H)$ . However, in the polydomain case, different parts of the JSV experience different flux density, which causes uneven current distribution with certain in-plane component. The latter does generate self-field, which depends on the current direction. This removes the mirror symmetry in the poly-domain case, as can be seen from Fig. 8.

### B. Half-flux quantum beatings in $I_c(H)$ modulation

The triplet current has a double-harmonic current-phase  $I_{tr}(\varphi)$  relation, Eq. (3), which leads to the half-flux quantum modulation period of  $I_{tr}(H)$ . However, this may be difficult to recognize in experiment because nano-scale JSV have not well-known demagnetization factors, especially if the total thickness  $2d_S + d_1 + d_N + d_2$  is comparable to the length  $L_x$  and the width  $L_y$  of the JSV. Presence of the demagnetization factor may significantly renormalize the modulation period of  $I_c(H)$ , which is not easy to quantify.

However, we note that a rather unambiguous qualitative signature of the triplet component appears in case of coexistence of singlet and triplet components of the supercurrent. This leads to appearance of small half-flux quantum beatings of  $I_c(H_x)$  with a flux-quantum period, as marked by the blue arrow [Fig. 8(d)]. Due to coexistence of the single-harmonic singlet and the double-harmonic triplet current, every second minimum of  $I_c(H_x)$  does not reach zero. Such beatings may also provide a quantitative information about relative amplitudes of singlet and triplet currents.

### C. Size dependence as a tool for identification of the triplet component

Finally, we return to the main question of this work, i.e., how to recognize the spin-triplet supercurrent from experimental characteristics of Josephson spin valves. The main fingerprint of the spin-triplet current is a characteristic asymmetric double maximum in field dependence on both sides of magnetostatically stable antiparallel state [see Fig. 3(a)]. However, from the presented analysis it follows that such a clear signature appears in  $I_c(H)$  modulation only for very small Josephson spin valves. With increasing JSV size it is distorted and becomes unrecognizable. The threshold length scales  $L_y^*$  of the order of 100 nm and  $L_x^* \lesssim 1 \mu\text{m}$  depend on materials and layer thicknesses.

There are two main obstacles for identification of the triplet supercurrent in large JSV: (i) appearance of ferromagnetic domains and (ii) flux quantization in applied magnetic field and a stray field from ferromagnetic layers.

Domains lead to removal of the pure antiparallel state, which determines the dip between the double maxima of  $I_{tr}(H)$ . As seen from Figs. 1(d), 5(d), and 7(d) the double maximum is progressively smeared and reduced in amplitude with increasing the number of domains and is completely washed away in the polydomain case. This is consistent with similar simulations made for three-layer  $\text{SF}_1\text{F}_2\text{F}_3\text{S}$  heterostructures [30]. A remaining single maximum of the triplet current

amplitude (see Fig. 8) is difficult to separate from a similar single maximum of the long-range singlet current amplitude [see Fig. 7(e)]. This complicates unambiguous identification of the triplet current in the polydomain case.

The size of the JSV affects both the domain structure and the flux quantization conditions. The larger is the JSV, the more domains there are and the less is the quantization field. As shown in Fig. 3(b), even in the monodomain case rapid oscillations of  $I_c(H)$  in large JSV may completely mask the double maxima of the triplet current amplitude.

Most clearly the triplet current can be identified in monodomain or few-domain JSV's (see Figs. 3 and 4). In those cases there is a well-defined antiparallel state of the spin valve, and the triplet current amplitude  $\propto \sin^2(\alpha)$  exhibits a characteristic double maximum on both sides of the AP state. However, this double maximum is distorted by flux quantization in large-size JSV's. In order to pinpoint the feature, we suggest the following strategy: (i) Systematic analysis of size dependence of  $I_c(H)$  characteristics of JSV's on the same chip. In this case, varying the JSV width  $L_y$  (perpendicular to the field) changes flux quantization conditions and thus allows identification of the underlying double maximum of the triplet current amplitude, as shown in Figs. 3 and 4. (ii) Clear observation of the triplet double maxima in the  $I_c(H)$  pattern requires the quantization field (significantly) larger than the coercive field. A comfortable way to increase the flux quantization field is to reduce the thickness of superconducting electrodes, which reduces the magnetic thickness [Eq. (6)] and increases the quantization field. Nb electrodes can be made as thin as 30–50 nm without major deterioration of superconducting properties. Even thinner  $d_S \sim 10$  nm films can be made of NbN films. The thinner the better it is for recognition of the triplet current. (iii) For confidence, it is advisable to confirm the alignment of the double-maximum edges with the edges of the antiparallel state by *in situ* probe of the AP state. As discussed in Ref. [26], this

can be done by measurement of high-bias magnetoresistance (AP state corresponds to maximum of resistance) and by *in situ* magnetometry (absolute fluxometry). In the latter case, the AP state is manifested by the well-defined intermediate AP step in the magnetization curve [see Figs. 1(a) and 4(a)]. The AP step is the most clear signature of the required monodomain (or few-) domain state. We emphasize that *in situ* measurements for the specific JSV are required. It is not enough to perform magnetization measurements of unpatterned multilayer films, which are always polydomain and have very different shape anisotropy compared to nanoscale JSV.

To conclude, the unconventional odd-frequency spin-triplet component of the supercurrent through a Josephson spin valve is manifested by a dissimilar double maximum on both sides of the antiparallel state of the spin valve. The robustness of this feature is directly linked to the robustness of the AP state. The magnetostatic stability of the AP state leads to the pronounced asymmetry of the maxima at the two sides of the AP state because the spin valve more easily goes into, rather than goes out of, the AP state. The stable AP state is achievable only in case of monodomains or few domains in the ferromagnetic layers and disappears in the polydomain case. Since the number of domains depends on the size of the JSV, nanoscale (submicron size) JSV's are required for analysis of the triplet current generation. We have shown that for the monodomain or few-domain JSV's it is possible to unambiguously identify the spin-triplet current by a systematic analysis of size and S-layer thickness dependencies of the critical current versus magnetic field modulation patterns, preferably in combination with *in situ* characterization of the studied spin valves.

#### ACKNOWLEDGMENT

Technical support from the Core Facility in Nanotechnology at Stockholm University is gratefully acknowledged.

- 
- [1] A. I. Buzdin, Proximity effects in superconductor-ferromagnet heterostructures, *Rev. Mod. Phys.* **77**, 935 (2005).
  - [2] F. S. Bergeret, A. F. Volkov, and K. B. Efetov, Odd triplet superconductivity and related phenomena in superconductor-ferromagnet structures, *Rev. Mod. Phys.* **77**, 1321 (2005).
  - [3] Ya. V. Fominov, A. A. Golubov, T. Yu. Karminskaya, M. Yu. Kupriyanov, R. G. Deminov, and L. R. Tagirov, Superconducting triplet spin valve, *JETP Lett.* **91**, 308 (2010).
  - [4] Ya. M. Blanter and F. W. J. Hekking, Supercurrent in long SFFS junctions with antiparallel domain configuration, *Phys. Rev. B* **69**, 024525 (2004).
  - [5] J. Kopu, M. Eschrig, J. C. Cuevas, and M. Fogelström, Transfer-matrix description of heterostructures involving superconductors and ferromagnets, *Phys. Rev. B* **69**, 094501 (2004).
  - [6] M. Houzet and A. I. Buzdin, Long range triplet Josephson effect through a ferromagnetic trilayer, *Phys. Rev. B* **76**, 060504 (2007).
  - [7] Y. Asano, Y. Sawa, Y. Tanaka, and A. A. Golubov, Odd triplet superconductivity and related phenomena in superconductor-ferromagnet structures, *Phys. Rev. B* **76**, 224525 (2007).
  - [8] L. Trifunovic, Z. Popovic, and Z. Radovic, Josephson effect and spin-triplet pairing correlations in SF1F2S junctions, *Phys. Rev. B* **84**, 064511 (2011).
  - [9] L. Trifunovic, Long-Range Superharmonic Josephson Current, *Phys. Rev. Lett.* **107**, 047001 (2011).
  - [10] A. S. Mel'nikov, A. V. Samokhvalov, S. M. Kuznetsova, and A. I. Buzdin, Interference Phenomena and Long-Range Proximity Effect in Clean Superconductor-Ferromagnet Systems, *Phys. Rev. Lett.* **109**, 237006 (2012).
  - [11] N. G. Pugach and A. I. Buzdin, Magnetic moment manipulation by triplet Josephson current, *Appl. Rev. Lett.* **101**, 242602 (2012).
  - [12] M. Alidoust, G. Sewell, and J. Linder, Non-Fraunhofer Interference Pattern in Inhomogeneous Ferromagnetic Josephson Junctions, *Phys. Rev. Lett.* **108**, 037001 (2012).
  - [13] I. I. Soloviev, N. V. Klenov, S. V. Bakurskiy, V. V. Bol'ginov, V. V. Ryazanov, M. Yu. Kupriyanov, and A. A. Golubov, Josephson magnetic rotary valve, *Appl. Phys. Lett.* **105**, 242601 (2014).
  - [14] I. I. Soloviev, N. V. Klenov, S. V. Bakurskiy, M. Yu. Kupriyanov, and A. A. Golubov, Critical current of SF-NFS Josephson junctions, *JETP Lett.* **101**, 240 (2015).

- [15] Y. Zhu, A. Pal, M. G. Blamire, and Z. H. Barber, Superconducting exchange coupling between ferromagnets, *Nat. Mater.* **16**, 195 (2017).
- [16] V. T. Petrashov, I. A. Sosnin, I. Cox, and A. Parsons, and C. Troadec, Giant Mutual Proximity Effects in Ferromagnetic/Superconducting Nanostructures, *Phys. Rev. Lett.* **83**, 3281 (1999).
- [17] J. Wang, M. Singh, M. Tian, N. Kumar, B. Liu, C. Shi, J. K. Jain, N. Samarth, T. E. Mallouk, and M. H. W. Chan, Interplay between superconductivity and ferromagnetism in crystalline nanowires, *Nat. Phys.* **6**, 389 (2010).
- [18] V. Pena, Z. Sefrioui, D. Arias, C. Leon, J. Santamaria, M. Varela, S. J. Pennycook, and J. L. Martinez, Coupling of superconductors through a half-metallic ferromagnet: Evidence for a long-range proximity effect, *Phys. Rev. B* **69**, 224502 (2004).
- [19] R. S. Keizer, S. T. B. Goennenwein, T. M. Klapwijk, G. Miao, G. Xiao, and A. Gupta, A spin triplet supercurrent through the half-metallic ferromagnet CrO<sub>2</sub>, *Nature (London)* **439**, 825 (2006).
- [20] T. Golod, A. Rydh, V. M. Krasnov, I. Marozau, M. A. Uribe-Laverde, D. K. Satapathy, Th. Wagner, and C. Bernhard, High bias anomaly in YBa<sub>2</sub>Cu<sub>3</sub>O<sub>7-x</sub>/LaMnO<sub>3+δ</sub>/YBa<sub>2</sub>Cu<sub>3</sub>O<sub>7-x</sub> superconductor/ferromagnetic insulator/superconductor junctions: Evidence for a long-range superconducting proximity effect through the conduction band of a ferromagnetic insulator, *Phys. Rev. B* **87**, 134520 (2013).
- [21] A. Singh, C. Jansen, K. Lahabi, and J. Aarts, High-Quality CrO<sub>2</sub> Nanowires for Dissipation-Less Spintronics, *Phys. Rev. X* **6**, 041012 (2016).
- [22] C. Richard, A. Buzdin, M. Houzet, and J. S. Meyer, Signatures of odd-frequency correlations in the Josephson current of superconductor/ferromagnet hybrid junctions, *Phys. Rev. B* **92**, 094509 (2015).
- [23] C. Bell, G. Burnell, C. W. Leung, E. J. Tarte, D.-J. Kang, and M. G. Blamire, Controllable Josephson current through a pseudospin-valve structure, *Appl. Rev. Lett.* **84**, 1153 (2004).
- [24] J. W. A. Robinson, G. B. Halász, A. I. Buzdin, and M. G. Blamire, Enhanced Supercurrents in Josephson Junctions Containing Nonparallel Ferromagnetic Domains, *Phys. Rev. Lett.* **104**, 207001 (2010).
- [25] B. Baek, W. H. Rippard, S. P. Benz, S. E. Russek, and P. D. Dresselhaus, Hybrid superconducting-magnetic memory device using competing order parameters, *Nat. Commun.* **5**, 3888 (2014).
- [26] A. Iovan, T. Golod, and V. M. Krasnov, Controllable generation of a spin-triplet supercurrent in a Josephson spin valve, *Phys. Rev. B* **90**, 134514 (2014).
- [27] Yu. N. Khaydukov, G. A. Ovsyannikov, A. E. Sheyerman, K. Y. Constantinian, L. Mustafa, T. Keller, M. A. Uribe-Laverde, Yu. V. Kislinskii, A. V. Shadrin, A. Kalaboukhov *et al.*, Evidence for spin-triplet superconducting correlations in metal-oxide heterostructures with noncollinear magnetization, *Phys. Rev. B* **90**, 035130 (2014).
- [28] J. W. A. Robinson, J. D. S. Witt, and M. G. Blamire, Controlled injection of spin-triplet supercurrents into a strong ferromagnet, *Science* **329**, 59 (2010).
- [29] T. S. Khaire, M. A. Khasawneh, W. P. Pratt, Jr., and N. O. Birge, Observation of Spin-Triplet Superconductivity in Co-Based Josephson Junctions, *Phys. Rev. Lett.* **104**, 137002 (2010).
- [30] N. Banerjee, C. B. Smiet, R. G. J. Smits, A. Ozaeta, F. S. Bergeret, M. G. Blamire, and J. W. A. Robinson, Evidence for spin selectivity of triplet pairs in superconducting spin valves, *Nat. Commun.* **5**, 3048 (2014).
- [31] V. A. Oboznov, V. V. Bol'ginov, A. K. Feofanov, V. V. Ryazanov, and A. I. Buzdin, Thickness Dependence of the Josephson Ground States of Superconductor-Ferromagnet-Superconductor Junctions, *Phys. Rev. Lett.* **96**, 197003 (2006).
- [32] N. G. Pugach, M. Yu. Kupriyanov, E. Goldobin, R. Kleiner, and D. Koelle, Superconductor-insulator-ferromagnet-superconductor Josephson junction: From the dirty to the clean limit, *Phys. Rev. B* **84**, 144513 (2011).
- [33] Yu. Khaydukov, R. Morari, O. Soltwedel, T. Keller, G. Christiani, G. Logvenov, M. Kupriyanov, A. Sidorenko, and B. Keimer, Interfacial roughness and proximity effects in superconductor/ferromagnet CuNi/Nb heterostructures, *J. Appl. Phys.* **118**, 213905 (2015).
- [34] M. Weides, Magnetic anisotropy in ferromagnetic Josephson junctions, *Appl. Phys. Lett.* **93**, 052502 (2008).
- [35] I. A. Golovchanskiy, V. V. Bol'ginov, V. S. Stolyarov, N. N. Abramov, A. Ben Hamida, O. V. Emelyanova, B. S. Stolyarov, M. Yu. Kupriyanov, A. A. Golubov, and V. V. Ryazanov, Micromagnetic modeling of critical current oscillations in magnetic Josephson junctions, *Phys. Rev. B* **94**, 214514 (2016).
- [36] T. Golod, A. Rydh, and V. M. Krasnov, Detection of the Phase Shift from a Single Abrikosov Vortex, *Phys. Rev. Lett.* **104**, 227003 (2010).
- [37] T. Golod, A. Iovan, and V. M. Krasnov, Single Abrikosov vortices as quantized information bits, *Nat. Commun.* **6**, 8628 (2015).
- [38] C. Klose, T. S. Khaire, Y. Wang, W. P. Pratt, Jr., N. O. Birge, B. J. McMorrán, T. P. Ginley, J. A. Borchers, B. J. Kirby, B. B. Maranville, and J. Unguris, Optimization of Spin-Triplet Supercurrent in Ferromagnetic Josephson Junctions, *Phys. Rev. Lett.* **108**, 127002 (2012).
- [39] A. I. Buzdin, A. S. Mel'nikov, and N. G. Pugach, Domain walls and long-range triplet correlations in SFS Josephson junctions, *Phys. Rev. B* **83**, 144515 (2011).
- [40] S. V. Bakurskiy, A. A. Golubov, N. V. Klenov, M. Yu. Kupriyanov, and I. I. Soloviev, Josephson effect in sifs tunnel junctions with domain walls in the weak link regio, *JETP Lett.* **101**, 765 (2015).
- [41] Simulations were performed using OOMMF software, <http://math.nist.gov/oommf/>.
- [42] R. Laiho, E. Lähderanta, E. B. Sonin, and K. B. Traito, Penetration of vortices into the ferromagnet/type-II superconductor bilayer, *Phys. Rev. B* **67**, 144522 (2003).
- [43] V. Vlasko-Vlasov, A. Buzdin, A. Melnikov, U. Welp, D. Rosenmann, L. Uspenskaya, V. Fratello, and W. Kwok, Domain structure and magnetic pinning in ferromagnetic/superconducting hybrids, *Phys. Rev. B* **85**, 064505 (2012).
- [44] J. C. Slonczewski, Conductance and exchange coupling of two ferromagnets separated by a tunneling barrier, *Phys. Rev. B* **39**, 6995 (1989).

- [45] R. L. Coren, Shape demagnetization effects in permalloy films, *J. Appl. Phys.* **37**, 230 (1966).
- [46] H. Chang and J. Burns, Demagnetizing and stray fields of elliptical films, *J. Appl. Phys.* **37**, 3240 (1966).
- [47] The intermediate step in the magnetization curve is absent because the two F layers in our case are not significantly different. The intermediate step, however, reappears even in the polydomain state when the two F layers are considerably different, i.e., one is soft and the other is hard (see, e.g., [25]).
- [48] V. M. Krasnov, V. A. Oboznov, and N. F. Pedersen, Fluxon dynamics in long Josephson junctions in the presence of a temperature gradient or spatial nonuniformity, *Phys. Rev. B* **55**, 14486 (1997).